PERFORMANCE OF GNSS/IMS INTEGRATION METHODS IN CONTEXT OF A NEAR REAL-TIME AIRBORNE MAPPING PLATFORM

KH. Gutjahr [a, *], P. Hafner [b], M. Ofner [a], K. Längauer [b], M. Wieser [b], N. Kühtreiber [b]

[a] Joanneum Research, Institute of Digital Image Processing, 8010 Graz, Austria - (karlheinz.gutjahr, martin.ofner)@joanneum.at
[b] Graz University of Technology, Institute of Navigation and Satellite Geodesy, 8010 Graz, Austria - petra.hafner@tugraz.at, wieser@geomatics.tu-graz.ac.at

Commission III, WG III/1

KEY WORDS: Mapping, GPS/INS, IMU, Rectification, Aerial, Multisensor

ABSTRACT:

The Institute of Digital Image Processing of the Joanneum Research has set up a low-cost airborne platform which provides high flexibility with respect to data acquisition and data processing. Applications being typically envisaged are mapping of disasters which often require near 'real-time' image processing. For the direct geo-referencing of each image, the parameters of the exterior orientation have to be determined with sufficient accuracy in real-time. Today the determination of the trajectory of a moving platform is increasingly based on the integration of satellite-based positioning and inertial measurement systems. The best GPS and IMU combination for the above mentioned application will be identified within a study of the Institute of Navigation and Satellite Geodesy of the Graz University of Technology. Within these tasks GPS receivers and IMUs of different quality and price classes are tested. In this paper preliminary results of the comprehensive investigation of diverse types of GNSS/IMS integration are presented. Moreover these results were used to analyse the 2D mapping potential of the low-cost airborne platform.

1. INTRODUCTION

The Institute of Digital Image Processing of the Joanneum Research (DIB) has set up a low-cost airborne platform which provides high flexibility with respect to data acquisition and data processing. Applications being typically envisaged are mapping of disaster events like flooding, land slides, storm damage, forest fires and the like. For such a disaster monitoring near 'real-time' image processing is frequently required, implying geo-referencing without using ground control points (GCPs) for optimization and validation purposes.

For the direct geo-referencing of each image the parameters of the exterior orientation – i.e., the position and the orientation of the camera at the moment of the exposure – have to be determined with sufficient accuracy in real time. Today the determination of the trajectory of a moving platform is increasingly based on the integration of satellite-based positioning and inertial measurement systems.

Global Navigation Satellite Systems (GNSS), such as GPS or the future Galileo system, represent absolute positioning (absolute coordinates of long-term accuracy), but in the sense of radio navigation, they are non-autonomous systems. In contrast, an inertial measurement system (use of gyroscopes and accelerometers) is self-contained, but is indicative of relative positioning (small coordinate differences of short-term accuracy). Therefore, the importance of such a sensor integration is obvious: an inertial measurement system (IMS) overcomes shadowing effects of GNSS, while GNSS compensates the IMS-typical drift behaviour (see Hofmann-Wellenhof et al. 2008, chap. 13.3.1).

The best GNSS and IMS combination for the above mentioned application will be identified within a study of the Institute of Navigation and Satellite Geodesy (INAS) of the Graz University of Technology. Within these tasks, GPS receivers and inertial measuring units (IMUs) of different quality and price classes are tested.

The type of integration depends on, besides the quality of the involved sensors, also on the coupling method within signal processing. Due to the used filtering technique, an uncoupled, a loosely coupled, and a tightly coupled integration of GPS receivers and IMUs can be performed. Depending on the chosen method, in a Kalman filter (optimal filter for stochastically non-stationary processes), either pre-processed data (in the uncoupled and loosely coupled cases) or raw data (for tightly coupled integration) are involved.

In this paper preliminary results of the comprehensive investigation of diverse types of GNSS/IMS integration are presented. Moreover these results were used to analyse the 2D mapping potential of the low-cost airborne platform.

2. LOW-COST AIRBORNE PLATFORM

The four key component groups of the presented airborne data acquisition and mapping platform (ADAM) are:
- so called 'professional' digital consumer cameras (for post-processing and/or near real-time ortho-images),
- a GPS phase receiver including in a final stage OmniSTAR (for the accurate determination of the position as part of the direct geo-referencing),
- an IMU mainly for the determination of the three Euler angles (orientation of the camera in space

---

* Corresponding author.

relative to true north and gravity) - as part of the direct geo-referencing,

- a PC for the data storage, the camera control and the necessary pre-processing (data reduction) on board of the aircraft before data transmission.

Besides the set-up and integration of all these hardware components, related software tools were developed for the data acquisition on board as well as the data processing on ground.

2.1 Imaging Unit

Currently, the imaging unit consists of three digital cameras:
- a digital Hasselblad camera with high resolution for post-processing ortho-images and 3D applications,
- a digital Canon camera with medium resolution for the data transmission and near real-time ortho-images and
- a FLIR thermal camera with low resolution – also for the data transmission and near real-time ortho-images.

The cameras are 'non metric' which means that their housing is not too bold and they are not calibrated concerning focal length and radiometry. But therefore costs are low. Nevertheless, the focal length and the lens distortion parameters can be determined during a block adjustment either measuring GCPs in flight or - more preferable - using lab calibration data. The missing radiometric calibration is of small influence on the mapping of natural hazards. The main camera characteristics of a typical platform set-up are summarized in Tab. 1 and Tab. 2.

An overview of the arrangement of the instruments of the data acquisition module is given in Fig. 3 and Fig. 4.

Camera	Resolution	Capture rate	Colour depth
Canon 30D	8 MPixel	0.25 Hz	8 Bit
H3D - 39	39 MPixel	0.25 Hz	16 Bit
Photon 640	0.3 MPixel	2.50 Hz	16 Bit

Table 1. Digital consumer cameras specifications.

Camera	Height above ground	Ground resolution	Covered area per image
Canon	300 m	10 cm	340 x 240 m^2
H3D - 39	300 m	5 cm	340 x 240 m^2
Canon	1000 m	32 cm	1130 x 800 m^2
H3D - 39	1000 m	16 cm	1130 x 800 m^2
Canon	2000 m	41 cm	2260 x 1600 m^2
H3D - 39	2000 m	32 cm	2260 x 1600 m^2

Table 2. Image parameters for a data capture with Hasselblad H3D - 39 and Canon camera.
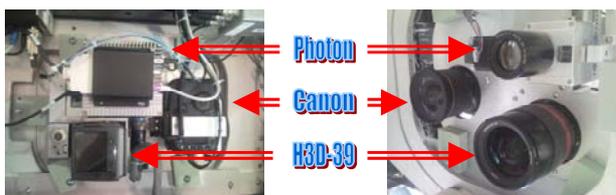

Figure 3. Instruments of the data acquisition module
(left: top view; right: bottom view).

Figure 4. Integration of ADAM into the pod of a DA42 MPP
(left: design; right: in flight operation).

2.2 Trajectory Determination

The direct georeferencing of each image depends on the determination of the position and the orientation of the camera at the moment of the exposure in real-time. To get the position and attitude, two hardware components are required: a GPS receiver for positioning and an IMU for the orientation of the camera. The best GNSS and IMS combination for the above mentioned application will be identified within the current study. Within these tasks, GPS receivers and IMUs of different quality and price classes are tested.

Investigated measurement systems (GNSS and IMS combinations)

INAS started to investigate GPS receivers and IMUs of different quality and price classes based on terrestrial field tests. In future, also measurement data based on airborne tests will be used, in order to provide a well-founded quality classification of GNSS and IMS combinations. The goal of the tests is to identify the best GNSS and IMS combination depending on the chosen application. The sensors as well as the type of the integration vary with their usage. For this reason, three different GPS receivers and three different IMUs are integrated in three different ways (uncoupled, loosely coupled, and tightly coupled, see Fig. 5).
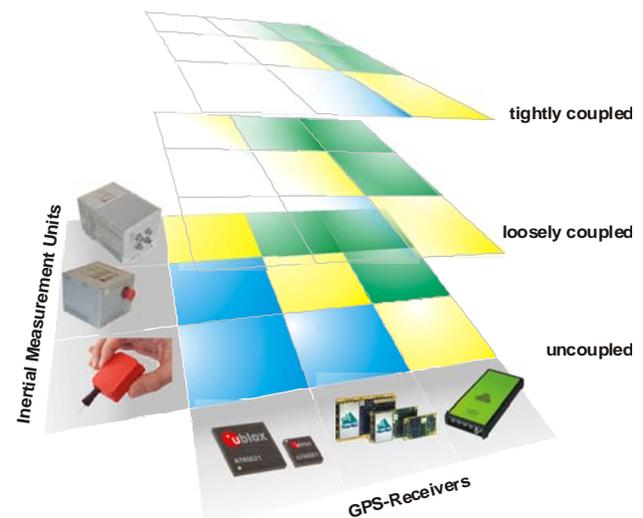

Figure 5. Different combinations of GPS receivers and IMUs of different quality and price classes.

For the investigations, the following GPS sensors are used in the integration process. They are listed in Tab. 6 with increasing quality and price (low, middle and high).

GPS sensor	type	update rate	position accuracy
MTi-G (Xsens)	L1	4 Hz	2.5 m
ProPak-V3 (NovAtel)	L1/L2	20 Hz	1 cm + 1 ppm
SigmaS (JAVAD)	L1/L2	100 Hz	1 cm + 1 ppm

Table 6. Characteristics of the GPS receivers.

Concerning the IMS component, the following sensors are tested. These three IMUs are representatives of low, middle, and high priced sensors. The attitude accuracies listed in Tab. 7 are specifications resulting from post-processing evaluations.

IMU	type	update rate	attitude accuracy	
			roll/ pitch	heading
MTi-G (Xsens)	MEMS	512 Hz	0.5 deg	1 deg
FSAS (iMAR)	FOG	200 Hz	0.008 deg	0.012 deg
iNAV-RQH (iMAR)	RLG	2000 Hz	0.005 deg	0.008 deg

Table 7. Characteristics of the IMUs.

In Tab. 6 as well as in Tab. 7 the same sensor MTi-G from Xsens can be found. The reason is that MTi-G is a system which contains accelerometers, gyroscopes and magnetometers together with a GPS receiver in one hardware housing. In this study this sensor is representative for a low price GNSS and IMS sensor.

Integration of GNSS and IMS

In the majority of cases, the commercial post processing evaluation software Inertial Explorer of the WAYPOINT Product Group of NovAtel is employed. Inertial Explorer enables the integration of GNSS and IMS data by applying a Kalman filter. The Kalman filter uses a dynamical model for the description of the movement of the vehicle. This circumstance declares the Kalman filter as an optimum filter for the integrated navigation. Concerning the Kalman filter, three different types of coupling can be distinguished: the uncoupled, the loosely coupled and the tightly coupled Kalman filter (see Hofmann-Wellenhof et al. 2003, pp. 289 – 291).

Uncoupled Kalman filter: In the case of an uncoupled Kalman filter, the GNSS as well as the IMS trajectory have to be evaluated separately. The input of the Kalman filter is on the one hand the position, the velocity and the time, based on GNSS measurements, and on the other hand the position, the velocity and the attitude, resulting from IMS measurements. The result of the integration depends, besides the types of measurements, on the accuracy of the computed GNSS and IMS trajectories and the performance of the dynamical model. The outputs of the filter are the integrated positions and velocities, while the attitude parameters and the time are not combined within the filter.

Loosely coupled Kalman filter: In contrast to the uncoupled Kalman filter, the output of the loosely coupled integration (position, velocity, and time) is used as support for the evaluation of the IMS trajectory. Identically to the uncoupled Kalman filter, the integration does not involve unprocessed measurement data. The GNSS as well as the IMS trajectory are

computed in advance; however, for the evaluation of the IMS trajectory, the output of the Kalman filter of the previous epoch is introduced as additional information (see Fig. 8). Among other facts, this method facilitates the computation of the initial position of the IMS trajectory and the correction of the drift.
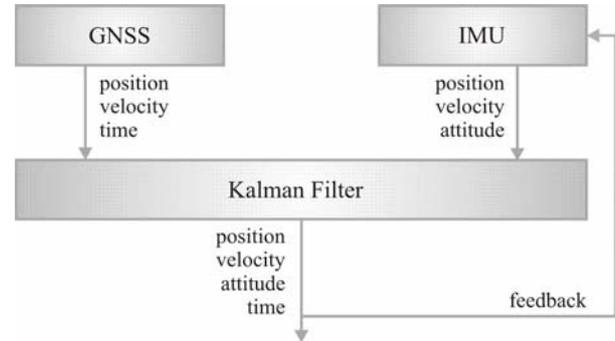

Figure 8. Scheme of a loosely coupled Kalman filter

Tightly coupled Kalman filter: In the case of the tightly coupled Kalman filter, there is no separated evaluation of the GNSS and IMS measurement data. As demonstrated in the scheme in Fig. 9, for the integration within the Kalman filter, the unprocessed measurement data (GNSS and IMS) are used. This method requires an adequate relationship between the GNSS and IMS observations. Among others, one advantage of the tightly coupled Kalman filter is that also GNSS position solutions with less than four satellites can be computed, since the absent observation is compensated by the complementary measurement system (IMS).
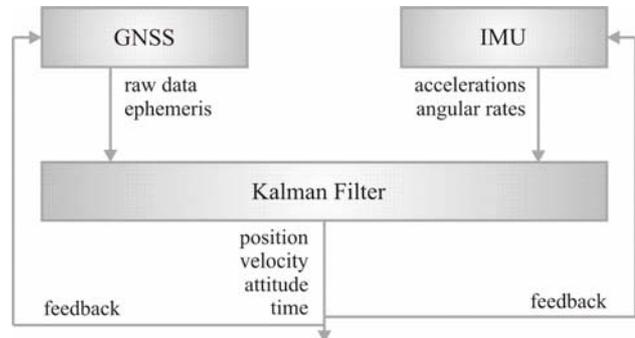

Figure 9. Scheme of a tightly coupled Kalman filter.

The loosely and the tightly coupling methods can be realized by using the Inertial Explorer of NovAtel. The integration with the uncoupled Kalman filter is not possible with the Inertial Explorer. This type of integration is done by a software which was designed and implemented at INAS. As input for the integration software also GNSS and IMS trajectories evaluated in Inertial Explorer can be used.

2.3 Near Real-time Mapping Workflow

For data acquisition on-board as well as data processing on-ground, DIB developed related software tools as follows (see Fig. 10):
On-board data processing:
- Triggering of cameras
- Data compression to reduce data volume

- Generation of ADAM data sets, comprising image data as well as associated information on camera position and exposition (GPS and IMU information)
- Interface to the on-board downlink unit.

On-ground data processing:
- Receipt of the transmitted ADAM data set in a data repository
- Data import activities including decompression of the image data
- Sequential ortho-rectification of the image data
- Optionally: image mosaicing of the individual ortho images
- Monitoring of the data acquisition campaign
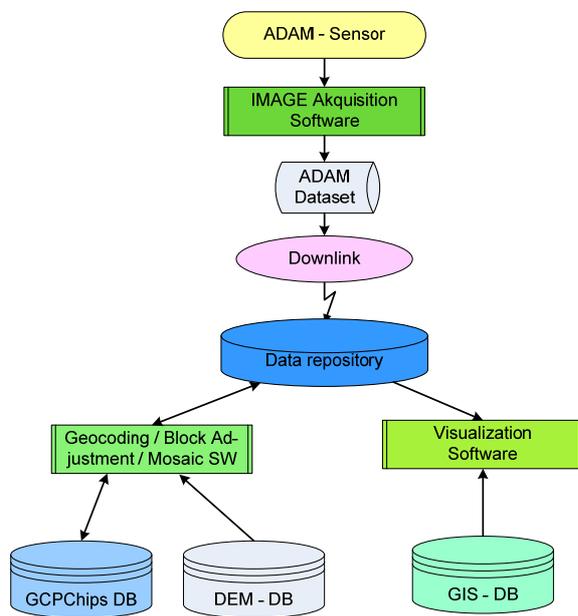- Visualization of ortho-rectified and mosaiced products.

Figure 10. Data acquisition and processing workflow.

According to the functionalities embedded in the ground processing station the key output products of this service are ortho-images and ortho-image mosaics in e.g. GeoTIFF format.

These products can be generated either in near real-time, usually at reduced geometric quality which is nevertheless supposed to be still sufficient in case of emergency situations, or in a post-processing scenario including options for geometric quality enhancement. Depending on the needs of the users, the products may be generated in alternative data formats. Additional products are in general feasible, based on dedicated data processing in order to automatically extract or highlight particular information contained in the data (hot spots, flooded areas, specifically endangered areas, etc.).

3. EXPERIMENTS

For disaster monitoring near 'real-time' image processing is frequently required, implying geo-referencing without using ground control points for optimization and validation purposes.

The components of the ADAM platform are designed in a way that a geo-location accuracy of less than 1 m is envisaged to be feasible at a flying height of 1000 m above ground.

In this chapter we show results of real data acquisition campaigns and give a theoretical proof of concept.

3.1 Current State

At the moment, the real-time trajectory determination can not use the OmniSTAR service which implies that the positioning accuracy of the platform is at least a factor 10 worse than in the envisaged final configuration. Nevertheless, the system was used several times for hazard mapping in Austria. One example of a near real-time ortho-image mosaic is shown in Fig. 11 (for further examples see Raggam et al., 2006 and Raggam et al., 2007).
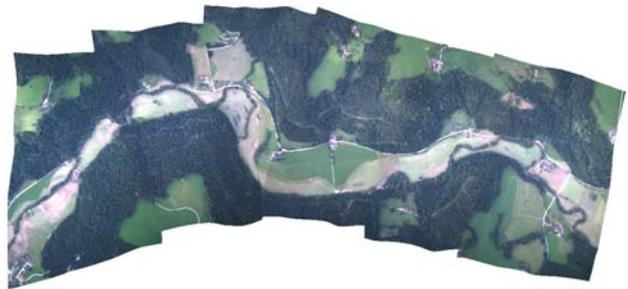

Figure 11. ADAM near real-time ortho image mosaic.

Visual inspections of the overlapping areas of sequent ortho-images and comparisons with reference maps show that the relative accuracy as well as the absolute accuracy is in the order of a few metres at maximum.

For many image acquisitions GCPs were identified in the images and the parameters of the exterior orientation were optimized using standard photogrammetric adjustment techniques. Tab. 12 shows one typical example out of these quality checks.

	Difference	ProPak/FSAS single point	Photogrammetric post-processing
X_0	0.828 m	± 1.252 m	± 0.517 m
Y_0	3.303 m	± 1.051 m	± 0.567 m
Z_0	4.041 m	± 1.369 m	± 0.164 m
ω	-0.063 deg	± 0.020 deg	± 0.031 deg
φ	0.117 deg	± 0.021 deg	± 0.035 deg
κ	-0.073 deg	± 0.087 deg	± 0.010 deg

Table 12. Comparison of the real-time and the photogrammetric post-processing solution of the parameters of the exterior orientation.

The first column summarizes the difference of the parameters of the exterior orientation between the GPS/IMS real-time solution and the results of the photogrammetric post-processing which is based on 43 GCPs measurements. Although the differences especially for the camera position seem at a first glance very large, they are well within the respective accuracy ranges.

3.2 Theoretical

The proof of concept is based on classical error propagation and thus we start with the basic (inverse) colinearity equations (Kraus, 1997, p. 15) which describe the relation between image coordinates and the respective object coordinates in the ground coordinate system:

$$X = X_0 - (Z - Z_0)\frac{r_{11}x + r_{12}y - r_{13}c}{r_{31}x + r_{32}y - r_{33}c}$$

$$Y = Y_0 - (Z - Z_0)\frac{r_{21}x + r_{22}y - r_{23}c}{r_{31}x + r_{32}y - r_{33}c} \quad (1)$$

where
c = focal length
x, y = image coordinates
X_0, Y_0, Z_0 = coordinates of the projection centre
X, Y, Z = object coordinates
r_{ij} = elements of the rotation matrix

As (1) are non-linear equations, a Taylor series expansion, neglecting coefficients of higher order, is applied to get the differential equations (linearisation):

$$dX = a_{11}dX_0 + a_{13}dZ_0 + a_{14}d\omega + a_{15}d\varphi + a_{16}d\kappa$$

$$dY = a_{21}dY_0 + a_{23}dZ_0 + a_{24}d\omega + a_{25}d\varphi + a_{26}d\kappa \quad (2)$$

Here we do not discuss the influence of inaccuracies in the modelling of the surface height. The law of error propagation in matrix notation is now:

$$Q_{xx} = A^T Q_{PP} A \quad (3)$$

where matrix A contains the coefficients a_{ij} of (2) and Q_{PP} is a diagonal matrix with the respective standard deviations of the camera position and rotation. It is sufficient to approximate the (planar) point error with the following ellipse:

$$a = \sqrt{\left(q_{xx}^2 + q_{YY}^2 + k\right)/2} \quad k = \sqrt{\left(q_{xx} - q_{YY}\right) + 4q_{xY}^2}$$

$$b = \sqrt{\left(q_{xx}^2 + q_{YY}^2 - k\right)/2} \quad \tan 2\varphi = 2q_{xY}/\left(q_{xx} - q_{YY}\right) \quad (4)$$

where
a, b = semi-major and semi-minor axis
φ = orientation angle

Fig. 14 shows the point error ellipses of the normal case for the standard deviations which can be found in the ProPak-V3/FSAS hardware specification. These specifications depend on the GNSS processing mode and are summarized in Tab. 13. Statistics about the semi-mayor axis of the calculated point error ellipses of the normal case are summarized in Tab. 15.

Looking at Tab. 15 it can be stated that a geo-location accuracy of better than 1 m is feasible for the post-processing solution and the real-time solution using the OmniSTAR service. Further numerical simulations show that a surface height error of 1.5 m would double the axes of the point error ellipses. However, the problem of the surface height can not be reduced to its absolute accuracy only, but it has to be seen in its spatial context. E.g., missing the roof of a building due to small position errors will

lead to disproportional large height errors and consequently large geo-location errors.

	ProPak/FSAS single point	ProPak/FSAS OmniSTAR	ProPak/FSAS post-processing
σ_{X_0}	1.20 m	0.10 m	0.02 m
σ_{Y_0}	1.20 m	0.10 m	0.02 m
σ_{Z_0}	1.80 m	0.15 m	0.05 m
σ_{ω}	0.015 deg	0.015 deg	0.008 deg
σ_{φ}	0.015 deg	0.015 deg	0.008 deg
σ_{κ}	0.041 deg	0.041 deg	0.012 deg

Table 13. Standard deviations used for the error propagation.
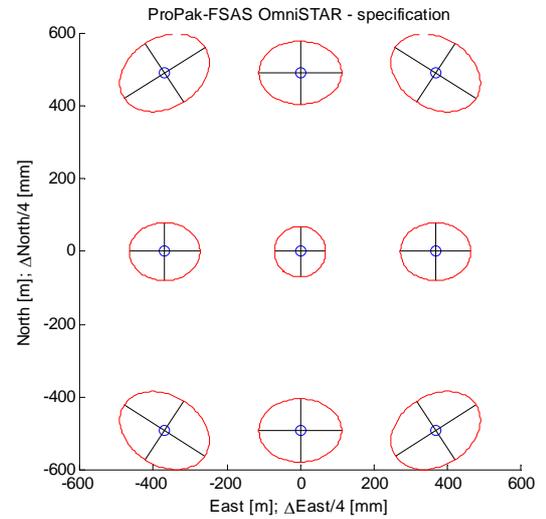

Figure 14. Point error ellipses for ProPak/FSAS OmniSTAR specification.

	ProPak/FSAS single point	ProPak/FSAS OmniSTAR	ProPak/FSAS post-processing
mean	1.532 m	0.449 m	0.438 m
min	1.228 m	0.280 m	0.263 m
max	1.674 m	0.523 m	0.513 m
std	0.160 m	0.085 m	0.088 m

Table 15. Semi-major axis of point error ellipse.

3.3 Terrestrial Sensor Test

For the terrestrial sensor test, four GPS antennas and three IMUs were mounted on a car, the corresponding GPS receivers were put inside the car (see Fig. 16). Different routes and manoeuvres were planed to cover various measurement conditions. At the moment, the measurements of the different hardware components in combination with the different integration types are analysed.

As the requirements for real-time mapping can not be fulfilled by the GPS/IMU sensor MTi-G from Xsens, this sensor is not considered in the detailed investigations here. Due to an acquisition problem the FSAS IMU data is excluded, too.
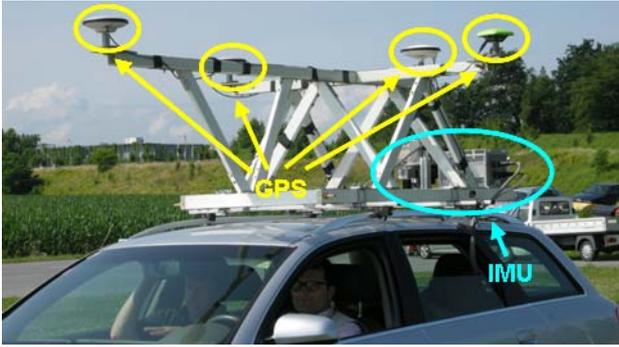
Figure 16. GPS/IMU platform mounted on a car

In the terrestrial sensor test, the most accurate results are achieved by using the IMU iNAV-RQH. To simulate airborne conditions, a test trajectory without GNSS signal obstructions was chosen. The results are based on the GPS receiver ProPak-V3 and the IMU iNAV-RQH which fulfil the requirements for real-time mapping as shown in the Fig. 17 and Fig. 18.

For alignment purposes the platform was at rest for the first 1000 seconds (120 s coarse alignment, 880 s fine alignment). The processing was done only in the forward direction to simulate real-time processing. The 1σ accuracy level of the estimated coordinates in a local level system is always below 2 cm (see Fig. 17). These values are estimated by the Kalman filter and might be a little bit too optimistic.
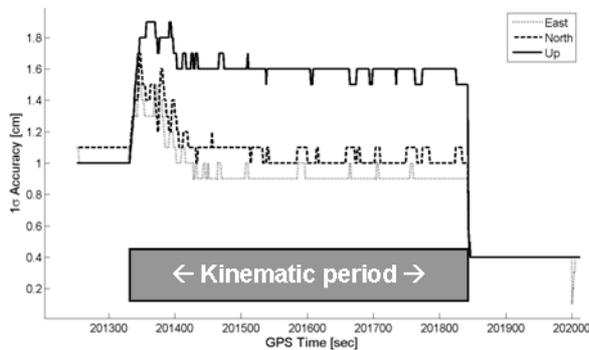

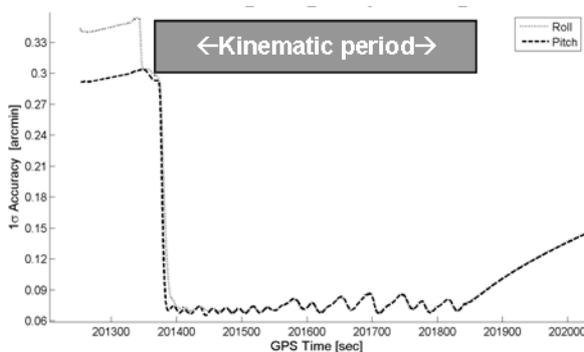Figure 17. Accuracy of the position of the loosely coupled integration (ProPak-V3, iNAV-RQH).

Figure 18. Accuracy of roll and pitch of the loosely coupled integration (ProPak-V3, iNAV-RQH).

Fig. 18 shows the 1σ accuracy levels for the roll and pitch attitude parameters which improve strongly at the beginning of

the kinematic period and stay below 0.1 arcsec afterwards. The results of the above described integration are representative since the use of the GPS receiver SigmaS from JAVAD did not significantly improve the results. The same is true for tightly coupling instead of loosely coupling. The reason is that no signal obstructions occur in the GPS measurement data.

4. CONCLUSION AND OUTLOOK

We presented the current and envisaged set-up of a low-cost airborne platform which provides high flexibility with respect to data acquisition and data processing. Practical as well as theoretical investigations showed that the system performance is within the expected accuracy ranges. To achieve the anticipated geolocation accuracy of better than 1 m, the integration of the OmniSTAR service is planned in the near future.

For further improvements concerning the GNSS and IMS integration, additional terrestrial field tests are planned. In order to check the results of the evaluation software (Inertial Explorer) a software which enables an uncoupled, loosely coupled and tightly coupled integration is and will be designed and implemented.

5. REFERENCES

Kraus, K. 1993. *Photogrammetry*. Vol. 1. Dümmler, Bonn

Raggam, H., Wack, R. & Gutjahr, K. 2006. Assessment of the Impact of Floods using Image Data acquired from a Helicopter. In *26th Earsel Symposium, "New Developments and Challenges in Remote Sensing"*, Warsaw, May 29th – June 2nd, 8 pages

Raggam, H., Wack, R. & Gutjahr, K. 2007. Mapping Capability of a Low Cost Aerial Data Acquisition Platform – First Results. In *ISPRS 2007 workshop Commission VI, WG VI/4 „High Resolution Earth Imaging for Geospatial Information"*, Hannover, May 29th - June 1st, 6 pages.

Hofmann-Wellenhof, B., Legat, K. & Wieser, M. 2003. *Navigation – Principles of positioning and guidance*. Springer, Wien NewYork.

Hofmann-Wellenhof, B., Lichtenegger, H. & Wasle, E. 2008. *GNSS – Global Navigation Satellite Systems*. Springer, Wien NewYork.

Websites (all last accessed 14 Jan. 2010):
iNAV-RQH:
http://www.imar-navigation.de/datenbl/nav_rqh_h_en.pdf
FSAS:
http://www.imar-navigation.de/datenbl/imu_fsas.pdf
Xsens:
http://www.xsens.com/images/stories/products/-PDF_Brochures/mti-g%20leaflet%2009.pdf
JAVAD-SigmaS:
http://www.javad.com/jgnss/products/receivers/sigma.html
NovAtel-ProPakV3:
http://www.novatel.com/Documents/Papers/ProPakV3.pdf

ACKNOWLEDGEMENT